

## Gyrokinetic simulations of spherical tokamaks

C M Roach<sup>1</sup>, I G Abel<sup>2</sup>, R J Akers<sup>1</sup>, W Arter<sup>1</sup>, M Barnes<sup>1,2</sup>, Y Camenen<sup>3</sup>,  
F J Casson<sup>3</sup>, G Colyer<sup>1</sup>, J W Connor<sup>1</sup>, S C Cowley<sup>1</sup>, D Dickinson<sup>4</sup>,  
W Dorland<sup>5</sup>, A R Field<sup>1</sup>, W Guttenfelder<sup>3</sup>, G W Hammett<sup>6</sup>, R J Hastie<sup>1</sup>,  
E Highcock<sup>2</sup>, N F Loureiro<sup>1</sup>, A G Peeters<sup>3</sup>, M Reshko<sup>4</sup>, S Saarelma<sup>1</sup>,  
A A Schekochihin<sup>2</sup>, M Valovic<sup>1</sup> and H R Wilson<sup>4</sup>

<sup>1</sup> EURATOM/UKAEA Fusion Association, Culham Science Centre, Abingdon, Oxfordshire, OX14 3DB, UK

<sup>2</sup> Rudolf Peierls Centre for Theoretical Physics, University of Oxford, 1 Keble Road, Oxford OX1 3NP, UK

<sup>3</sup> CFSA, Department of Physics, University of Warwick, Coventry CV4 7AL, UK

<sup>4</sup> Department of Physics, University of York, Heslington, York, YO10 5DD, UK

<sup>5</sup> University of Maryland, College Park, MD, USA

<sup>6</sup> Princeton Plasma Physics Laboratory, Princeton University, NJ, USA

Received 29 June 2009, in final form 20 August 2009

Published 11 November 2009

Online at [stacks.iop.org/PPCF/51/124020](http://stacks.iop.org/PPCF/51/124020)

### Abstract

This paper reviews transport and confinement in spherical tokamaks (STs) and our current physics understanding of this that is partly based on gyrokinetic simulations. Equilibrium flow shear plays an important role, and we show how this is consistently included in the gyrokinetic framework for flows that greatly exceed the diamagnetic velocity. The key geometry factors that influence the effectiveness of turbulence suppression by flow shear are discussed, and we show that toroidal equilibrium flow shear can sometimes entirely suppress ion scale turbulence in today's STs. Advanced nonlinear simulations of electron temperature gradient (ETG) driven turbulence, including kinetic ion physics, collisions and equilibrium flow shear, support the model that ETG turbulence can explain electron heat transport in many ST discharges.

(Some figures in this article are in colour only in the electronic version)

### 1. Introduction

Data from the IMA-scale experiments MAST and NSTX are unveiling the nature of plasma confinement in spherical tokamaks (STs) [1, 2]. Neutral beam injection (NBI) drives strong toroidal flow in these devices, and radial shear in the component perpendicular to the magnetic field acts to twist the turbulent eddies that may be responsible for anomalous transport. Perpendicular flow shear is characterized by the parameter  $\gamma_E = dV_\perp/dr$ , where  $1/\gamma_E$  corresponds to the time for a turbulent eddy to be tilted by  $45^\circ$  in the plane perpendicular to the magnetic field. This twisting of turbulent eddies competes with and potentially disrupts the linear instability drive, and when  $\gamma_E$  exceeds the linear growth rates, it can suppress

turbulence [3, 4]. The parallel component of the sheared toroidal flow, on the other hand, provides a linear drive that can enhance the turbulence. We show that equilibrium geometry at mid-radius in STs favours the suppression of turbulence by the perpendicular component of the sheared toroidal flow. In section 2 we review our current physics understanding of plasma transport in STs, and highlight the important role of equilibrium flow shear in regulating the more slowly growing longer wavelength modes. Equilibrium flow shear can be accommodated in the gyrokinetic framework, as outlined in section 3, and has recently been implemented and tested in local gyrokinetic codes, GS2 [5] and GWK [6]. Linear gyrokinetic simulations demonstrate that, at mid-radius in MAST, the typical experimental level of  $\gamma_E$  stabilizes ion temperature gradient (ITG) driven modes, and leaves the faster growing electron temperature gradient (ETG) driven modes unstable. Section 4 assesses the influence of flow shear on nonlinear simulations of ETG turbulence that have predicted significant electron heat transport in MAST [7], and probes the robustness of that important result using more sophisticated gyrokinetic models that include flow shear, and which also include kinetic ions and collisions. A summary of the main conclusions is presented in section 5. In appendix A, we demonstrate close agreement between local microstability results from three gyrokinetic codes, in the collisionless electrostatic limit without equilibrium flow shear, for a strongly shaped MAST outer equilibrium flux-surface.

## 2. Confinement, transport and gyrokinetic studies of STs

The measured energy confinement time,  $\tau_E$ , in MAST and NSTX is broadly consistent with the ITER IPB98(y,2) scaling law,  $\tau_E = 0.0562 I_p^{0.93} B_\phi^{0.15} P_L^{-0.69} n^{0.41} M^{0.19} R^{1.97} (a/R)^{0.58} \kappa^{0.78}$  [8], derived from conventional aspect ratio devices, where  $\tau_E$ , plasma current  $I_p$ , toroidal field  $B_\phi$ , loss power  $P_L$ , density  $n$ , mean ion mass number  $M$  and major radius  $R$  are in units s, MA, T, MW,  $10^{19} \text{ m}^{-3}$ , amu and m, respectively,  $a/R$  is the inverse aspect ratio and  $\kappa$  is the elongation. Detailed parameter scans, however, indicate that confinement scales differently in STs [2, 9], and the MAST scaling in terms of engineering parameters,  $\tau_E = 0.186 I_p^{0.59} B_\phi^{1.4} P_L^{-0.73}$  depends more weakly on  $I_p$  and more strongly on  $B_\phi$  [9]. This scaling, favourable for future ST devices, is not yet understood. NSTX finds a similar scaling and attributes the improvement of  $\tau_E$  to (i) a reduction in transport in the (dominant) electron channel with increasing  $B_\phi$  and (ii) falling neoclassical ion heat transport with increasing  $I_p$  [2]. We note that the impact of strong toroidal flows on energy confinement is not clearly isolated in these scaling laws—and perhaps it should be. In any tokamak plasma heated by toroidally injected NBI (such as MAST and NSTX), toroidal momentum and energy confinement times can be shown to be related via  $\tau_\phi \sim M_\phi (v_b/v_{ti}) \tau_E$ , where  $M_\phi = V_\phi/v_{ti}$  is the toroidal Mach number,  $V_\phi$  is the toroidal flow and  $v_b$ ,  $v_{ti}$  are the velocities of beam and thermal ions, respectively. In MAST,  $M_\phi \sim 0.4$  and  $v_b/v_{ti} \sim \sqrt{60}$ , which implies  $\tau_\phi \sim 3\tau_E$ . The fact that  $\tau_\phi$  is closely linked to ion confinement suggests that, for these MAST conditions, ion energy is better confined than electron energy and that energy losses arise predominantly through the electron channel.

Both MAST and NSTX have frequently observed the suppression of anomalous ion heat transport, with the measured ion thermal diffusivity  $\chi_i$  approaching the neoclassical prediction  $\chi_i^{\text{nc}}$ , while the experimental electron thermal diffusivity  $\chi_e$  is usually much larger [2, 10]. Analysis of ion channel internal transport barriers in co-NBI MAST plasmas suggests that these arise as a result of the sheared flow suppression of ITG turbulence [10]. Transport analysis of similar L- and H-mode MAST plasmas [10] for  $r/a > 0.5$  revealed  $\chi_i \sim \chi_i^{\text{nc}}$  and  $\chi_e \sim (2-4)\chi_i^{\text{nc}}$  in H-mode; however, both  $\chi_i$ ,  $\chi_e > \chi_i^{\text{nc}}$  in L-mode<sup>7</sup>. The trapped-gyro-Landau

<sup>7</sup> Data from the MAST discharges in [10] are available through the 2008 public release of the ITPA international multi-tokamak confinement profile database [11].

fluid (TGLF) model for anomalous transport [12] is applicable to shaped, low  $R/a$  plasmas, and first comparisons with MAST and NSTX data [13] also suggest that sheared flow plays a vital role in stabilizing ITG turbulence. For the MAST and NSTX plasmas analysed, the TGLF model predicts that  $\chi_i \sim \chi_i^{\text{nc}}$  over a significant fraction of the minor radius, and that ETG turbulence dominates the electron heat flux,  $q_e$ , for safety factor  $q > 1$ , but overestimates  $T_e$  in the core. In the MAST L-mode discharge #8505 [10], where ion heat transport was anomalous, ITG turbulence was modelled, without flow shear<sup>8</sup>, using the global gyrokinetic particle-in-cell code ORB5 [14]. In the gradient zone the nonlinearly saturated  $\chi_i$  was found to be significantly larger than the measured value, indicating the importance of including flow shear in the modelling of ion scale turbulence in MAST. Radial shear of the diamagnetic equilibrium flow is stronger in STs than at conventional aspect ratio, and gyrokinetic calculations have previously suggested that this should benefit performance in future ST burning plasma devices [15].

Gyrokinetic simulation for STs faces a number of challenges: (i) the gyrokinetic expansion parameter  $\delta = \rho_i/L$  is not very small ( $\rho_i/L \sim 0.02$  in MAST, where  $\rho_i$  is the ion Larmor radius and  $L$  is the equilibrium length scale); (ii) highly shaped, low aspect ratio plasmas rule out simple analytic equilibrium models; (iii) magnetic perturbations can be important if  $\beta$  is large; (iv) there are strong toroidal flows with  $M_\phi \sim 1$ ; (v) radially sheared flows impact on microturbulence and (vi) there can be significant populations of super-Alfvénic fast particles. Gyrokinetic codes are rising to meet many of these challenges: [appendix A](#) demonstrates close agreement in electrostatic microstability results from three local flux-tube gyrokinetic codes (GKW, GS2 and GYRO [16]) for a typical strongly shaped MAST equilibrium flux surface. Microinstability based transport mechanisms in STs have been explored using linear studies (mainly with GS2 and GYRO). The effect of including the magnetic field perturbation,  $\delta B$ , was found, using GS2, to be significant at mid-radius in MAST [17, 18], where locally  $\beta \sim 0.1$ : at  $k_\perp \rho_i \lesssim 1$ , where  $k_\perp$  is the perpendicular wavenumber, electromagnetic modes dominated over ITG modes, and these exhibited tearing and twisting parity in the H-mode and L-mode plasmas, respectively; furthermore including  $\delta B_\parallel$  reduced the growth rates of ETG instabilities [18]. A detailed study of microtearing modes found that they are not peculiar to the ST and that their growth rate is sensitive to  $dT_e/dr$ , magnetic drifts and  $v_{*e}$  [19]. Microtearing modes have since been found in conventional aspect ratio tokamak plasmas [20, 21], and a nonlinear theoretical estimate of microtearing mode saturation was found to be consistent with NSTX measurements of  $\chi_e$  [22]. Electron heat transport was observed to increase dramatically with rising beam power in the core of NSTX, where fast particle instabilities were observed and thermal temperature gradients were too low to drive transport via the usual mechanisms [23]. Microtearing modes, fast particle instabilities and sonic flows will not be addressed further in this paper.

GS2 microstability analyses of MAST discharges, without flow shear, have revealed that the sheared flow stabilization criterion  $\gamma_E = r/q \, d(qv_E/r)/dr > \gamma_{\text{max}}$  [4] (where  $v_E$  is the equilibrium  $E \times B$  velocity and  $\gamma_{\text{max}}$  is the maximum linear growth rate) is often satisfied for ITG but not ETG modes in MAST plasmas [17, 18]. Nonlinear calculations for STs have therefore generally focussed on modelling ETG turbulence. GS2 simulations (without flow shear) for a typical H-mode plasma, suggest that ETG can carry significant electron heat flux at mid-radius in MAST [7], consistent with findings from GYRO simulations for NSTX [2]. In this paper flow shear will be included self-consistently in local gyrokinetic simulations, to assess more thoroughly the impact of flow shear on ITG and ETG turbulence in MAST.

<sup>8</sup> The TGLF model predicts that flow shear partly suppresses ITG turbulence in this plasma.

### 3. Gyrokinetics with equilibrium flow shear

We now describe how equilibrium flow shear can be accommodated in the gyrokinetic equation (GKE) that describes microinstabilities. Equilibrium flows in tokamaks are divergence free and can be expressed in a general form in terms of components that are toroidal and parallel to the magnetic field:

$$\mathbf{V} = R\Omega(\psi)\mathbf{e}_\phi + K(\psi)\mathbf{B} \quad (1)$$

where the toroidal angular frequency  $\Omega$ , and  $K$  are functions of poloidal flux  $\psi$ .

$\mathbf{V}$  has contributions from diamagnetic flows,  $v_{\text{dia}} \sim \frac{\rho_i}{L} v_{\text{ti}}$ , and the equilibrium  $\mathbf{E} \times \mathbf{B}$  flow,  $v_E$ , which can approach  $v_{\text{ti}}$ . A neoclassical parallel equilibrium flow, driven by radial gradients and constrained by collisions, largely cancels any other poloidal flow: the poloidal component of  $v_E$  is entirely compensated by the neoclassical parallel flow, but for the diamagnetic flow this cancellation is incomplete in the presence of an ion temperature gradient. Here we consider only flows that are dominated by  $v_E$  and exceed the diamagnetic flow velocity (i.e.  $V \gg \frac{\rho_i}{L} v_{\text{ti}}$ ). These strong flows are toroidal (i.e.  $K(\psi) = 0$  in equation (1)), and consistent with the ST equilibria that we will investigate. The criterion for equilibrium flow shear to suppress turbulence requires  $V/L_V \sim O(v_{\text{ti}}/L)$ , where  $L_V$  is the gradient scale length associated with the flow. For the case of strong flows assumed here, turbulence can be suppressed by flow shear with  $L_V \gg \rho_i$ . It should be noted that for weaker diamagnetic flows this is only possible if  $L_V \sim O(\rho_i)$ , which overstretches the gyrokinetic orderings.

The GKE for the leading order, nonadiabatic piece of the perturbed guiding centre distribution,  $g$ , with sonic toroidal flows  $\mathbf{V} = R\Omega(\psi)\mathbf{e}_\phi$  appears in [24] as equation (56). We assume the toroidal flow contribution dominates the radial electric field, and take  $V = R\Omega(\psi) \sim O(M_\phi v_{\text{ti}})$ . Expanding to leading order in  $M_\phi$  (where  $\rho_i/L < M_\phi < 1$ ) while retaining locally steep radial rotation gradients by ordering  $\partial\mathbf{V}/\partial r = R^2 B_p \Omega' \mathbf{e}_\phi \sim O(v_{\text{ti}}/L)$  (where  $'$  denotes  $d/d\psi$ , and  $B_p$  is the poloidal magnetic field strength), and dropping nonlinear and magnetic perturbation terms for brevity, yields the linear electrostatic GKE with subsonic sheared toroidal flow:

$$\left( \frac{\partial}{\partial t} + \mathbf{V} \cdot \nabla_\perp \right) g + (c_\parallel \mathbf{b} + c_{D0}) \cdot \nabla_R g = -\frac{qJ_0}{m} \frac{\partial F}{\partial \epsilon} \left( \frac{\partial}{\partial t} + \mathbf{V} \cdot \nabla_\perp \right) \tilde{\Phi} - \frac{qJ_0}{m\Omega_c} \mathbf{b} \times \nabla_R \tilde{\Phi} \cdot \nabla_R F + \frac{qJ_0}{m\Omega_c} \frac{\partial F}{\partial \epsilon} \mathbf{b} \times \nabla_R \tilde{\Phi} \cdot \left[ c_\parallel R\Omega' \frac{B_\phi}{B} \nabla \psi \right], \quad (2)$$

where the guiding centre velocity  $\mathbf{v} = \mathbf{V} + \mathbf{c}$ ,  $\Omega_c$  is the cyclotron frequency,  $c_{D0} = \mathbf{b} \times (c_\perp^2/2 \nabla \log B + c_\parallel^2 \mathbf{b} \cdot \nabla \mathbf{b})/\Omega_c$  contains the magnetic drifts,  $\mathbf{V} = (R\Omega_0 + R\Omega'(\psi - \psi_0))\mathbf{e}_\phi$ ,  $F = A(\psi)e^{-m\epsilon/T(\psi)}$  is the isotropic equilibrium distribution function in the co-moving frame,  $J_0$  is the Bessel function with argument  $z = k_\perp c_\perp/\Omega_c$  and  $\epsilon = c_\parallel^2/2 + c_\perp^2/2$ . The  $\mathbf{V} \cdot \nabla$  terms and the last term that is proportional to  $\Omega'$  are due to sheared toroidal flow. The  $\mathbf{V} \cdot \nabla_\perp$  terms act to differentially advect perturbations. In a local flux tube,  $\Omega_0$  appears as a Doppler shift in the perturbation frequency, and in codes, such as GS2 and GKW, where FFTs are used in the radial direction (denoted by  $x$ ), the radial shearing term is implemented by forcing  $k_x$  to depend linearly on time [25] to satisfy  $dk_x/dt = \gamma_E k_y$ , where the equilibrium flow shearing rate  $\gamma_E = \frac{\rho}{q} \frac{d\Omega}{d\rho}$  and  $\rho$  is a radial flux surface label. (Equivalently in ballooning space the shearing term is implemented by making the ballooning parameter  $\theta_0$  depend linearly on time.) The final term on the RHS of equation (2) is the linear drive from the parallel component of the sheared toroidal rotation, and this is fully determined by geometry,  $\gamma_E$  and the perturbations. This term is proportional to the following product of  $\gamma_E$  and a geometrical factor:

$$-\frac{qRB_\phi}{\rho B} \gamma_E \sim -\frac{B_\phi}{B_p} \gamma_E \text{ at large aspect ratio.}$$

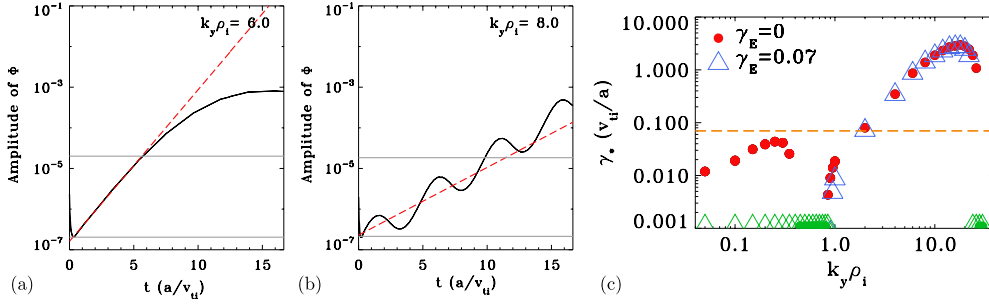


**Figure 1.**  $\Phi$  amplitude versus  $t$  in linear electrostatic calculations for a mid-radius surface in MAST for (a)  $k_y \rho_i = 6$ ,  $\gamma_E = 0.07 v_{ti}/a$  and (b)  $k_y \rho_i = 8$ ,  $\gamma_E = 0.5 v_{ti}/a$ . Horizontal grey lines indicate the amplitude range used to obtain the effective growth rate  $\gamma_*$ . (c)  $\gamma_*$  versus  $k_y \rho_i$  for  $\gamma_E = 0$  (circles) and  $\gamma_E = 0.07 v_{ti}/a$  (triangles). The horizontal dashed line shows the level of  $\gamma_E$ . Symbols at the  $\gamma_*$ -axis minimum (i.e. at  $\gamma_* = 0.001 v_{ti}/a$ ) denote stable modes.

It is stronger for ions than electrons as it is also proportional to  $\sqrt{m}$ , where  $m$  is particle mass. The implementation of the parallel flow shear linear drive term in GS2 shows excellent agreement with analytic theory for the radially sheared parallel flow instability in slab geometry without magnetic shear.

### 3.1. Linear impact of flow shear on MAST

Linear gyrokinetic microstability calculations for a typical mid-radius flux surface in MAST were performed in ballooning space using GS2, and here we indicate how effective growth rates were obtained. At finite  $\gamma_E$ , a linear eigenfunction cannot strictly be represented by a ballooning mode with a specific single choice of the ballooning parameter  $\theta_0$ . Ballooning modes labelled by  $\theta_0$  can only be considered to be independent at  $\gamma_E = 0$ , as flow shear couples modes with different  $\theta_0$ . With infinitesimal flow shear, the true linear eigenmode can be constructed as an ensemble of ballooning modes and the growth rate becomes the  $\theta_0$ -averaged growth rate in the absence of flow shear,  $\langle \gamma \rangle_{\theta_0}$  [26]. It is still, however, useful to consider the evolution of a pure ballooning mode with specified initial  $\theta_0$  at  $t = 0$ : its  $\theta_0$  will evolve linearly in time and its amplitude will grow as  $e^{(\langle \gamma \rangle_{\theta_0} + C(t))t}$ , where  $C(t)$  is oscillatory (i.e. it is a Floquet mode). An example of such growth is illustrated in figure 1(b). Linear theory is only ever applicable up to the finite amplitude where nonlinear physics becomes important, and from any initial state with finite amplitude turbulence due to noise, this nonlinear threshold may be reached after a finite mode amplification. The crucial point here is that, even when the true linear eigenmode is stable for  $\gamma_E < \gamma_{\max}$ , a pure ballooning mode with specified  $\theta_0$  can still experience many linear growth times and reach the nonlinear threshold *before* the ballooning parameter is affected by flow shear<sup>9</sup>.

It is straightforward to specify a prescription for obtaining an *effective* linear growth rate  $\gamma_*$  for a pure ballooning mode with a particular choice of  $k_y$ . In an initial value code such as GS2, it is sufficient to track the amplitude of the mode, following the associated evolution in  $\theta_0(t)$ . We adopt the following simple model to determine the effective linear growth rate  $\gamma_*$ : (i) specify a finite mode amplification factor  $F_{\text{NL}}$  (here we set  $F_{\text{NL}} = 100$ ), (ii) when/if a mode becomes amplified by  $F_{\text{NL}}$ , we consider it unstable and ignore subsequent linear evolution, (iii) determine  $\gamma_*$  by fitting  $\Phi(k_y, \theta_0(t), t)$  over the range of  $t$  that achieved the required mode

<sup>9</sup> A related discussion for grofluid calculations with flow shear in ballooning space is given in [27].

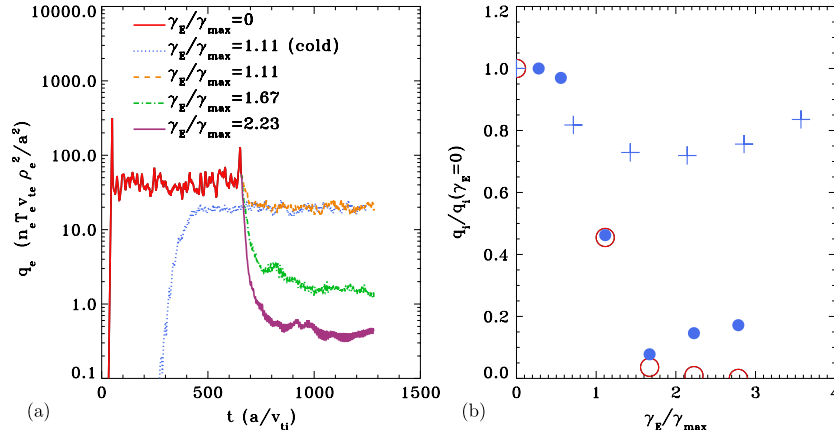


**Figure 2.** (a) Electrostatic GS2 simulations for the cyclone parameters described for various levels of  $\gamma_E/\gamma_{\max}$ , without the parallel flow shear linear drive term, showing  $q_i$  versus  $t$ . In (b) the ratio of saturated  $q_i$  to that with  $\gamma_E = 0$  is plotted versus  $\gamma_E/\gamma_{\max}$ : circles show GS2 results for the cyclone equilibrium described with (solid) and without (open) the parallel flow shear linear drive term and GKW results with the parallel flow shear linear drive term for the standard case of [28] (crosses).

amplification, starting from an initial minimum in the amplitude. This procedure is illustrated in figures 1(a) and (b), and was followed to obtain the mid-radius MAST growth rate spectra in figure 1(c) for  $\gamma_E = 0$  and for  $\gamma_E = 0.07v_{ti}/a$ .

Figure 1(c) clearly illustrates, using linear results from GS2, that ITG modes ( $k_y \rho_i < 1$ ) at mid-radius in MAST can be stabilized by a conservative level of  $\gamma_E$ , while more rapidly growing ETG modes remain unstable.

### 3.2. Nonlinear ITG simulations with flow shear for large aspect ratio plasmas

Nonlinear calculations of ITG turbulence assuming adiabatic electrons (AEs) and including equilibrium flow shear, have been carried out with GS2 and GKW, both for circular cyclone [29] plasma equilibrium parameters ( $R/a = 3$ ,  $r/a = 0.54$ ,  $q = 1.39$ ,  $\hat{s} = (r/q) dq/dr = 0.8$ ,  $\beta = \beta' = 0$ ,  $R/L_{T_i} = 6.9$ ,  $R/L_n = 2.2$ ,  $T_i = T_e$ ) and for the slightly different standard case of [28] with  $q = 2$ ,  $\hat{s} = 1.0$  and  $r/a = 0.5$ . These simulations included 16 modes in the binormal perpendicular wavenumber that span  $0.05 < k_y \rho_i < 0.75$ , and were carried out for different levels of  $\gamma_E$ , both with and without the linear drive term. Convergence tests, using GKW with more binormal modes, found that the 16 mode simulations were well resolved in the presence of turbulence. Simulations with finite  $\gamma_E$  were performed either: (i) as warm-starts from the saturated state of the  $\gamma_E = 0$  simulation or (ii) as cold-starts from low amplitude noise. The same saturated ion heat flux  $q_i$  was reached in either scenario, as illustrated for  $\gamma_E/\gamma_{\max} = 1.11$  in figure 2(a). GS2 results in figure 2(b) show that without the sheared parallel flow linear drive term,  $q_i$  is increasingly suppressed as the flow shear increases in strength, and becomes fully suppressed close to  $\gamma_E/\gamma_{\max} \sim 2$  (as was found in [28]). When the sheared parallel flow linear drive is included (see the results that appear as crosses and filled circles in figure 2(b)),  $q_i$  falls with increasing flow shear at low  $\gamma_E$  to a minimum where it is not fully suppressed, and starts to increase with  $\gamma_E$  above  $\gamma_E/\gamma_{\max} \sim 1.5$ . Figure 2(b) shows that turbulence suppression is much more modest for the standard case parameters of [28] than for the cyclone parameters. The parallel flow shear linear drive term is stronger in the former equilibrium, where the geometrical factor  $qR/r$  (corresponding to  $B_\phi/B_p$ ) is larger:

$qR/r = 12$  in the standard case of [28] and 7.7 in the cyclone equilibrium. The GKW results for the standard case of [28] are consistent with [28]. Parallel flow shear both enhances the growth rate of ITG modes [30] and drives its own instability when  $U'_{\parallel} L_n / (\sqrt{2} v_{ti}) > 1$  [31], where  $U'_{\parallel} = R\Omega' B_{\phi} / B$  if the equilibrium flow is toroidal, as here. For the standard case of [28] this criterion predicts a parallel flow shear driven instability (without perpendicular flow shear) for  $\gamma_E / \gamma_{\max} \gtrsim 0.5$ : i.e. the parallel shear driven mode should be unstable in most of the simulations that are marked as blue crosses in figure 2(b). For the cyclone equilibrium where the linear drive is smaller (blue solid circles in figure 2(b)), this instability is predicted at higher values of  $\gamma_E$ , where the turbulence has become more strongly suppressed by the perpendicular component of the flow shear.

It is interesting to note that at mid-radius in STs the factor  $qR/r$  is smaller: e.g. at mid-radius in MAST  $qR/r \sim 4$ . Given that the parallel flow shear linear drive is reduced at lower  $qR/r$  and/or  $B_{\phi}/B$ , shear flow suppression of turbulence is clearly favoured at mid-radius in STs where both of these geometrical factors are smaller than in conventional devices. Turbulence suppression is favoured here because the component of toroidal flow that is perpendicular to the magnetic field is larger, owing to the higher ratio  $B_p/B_{\phi}$ .

#### 4. Improved nonlinear ETG simulations for MAST

Figure 1(c) showed that, at mid-radius in MAST, ITG modes are linearly suppressed by flow shear, while ETG modes are unaffected: we now explore the significance of ETG turbulence. Fully electromagnetic simulations with GS2, neglecting  $\gamma_E$ , demonstrated that the electron heat flux from ETG turbulence can be experimentally significant at mid-radius in MAST [7]. The reference model in [7] assumed adiabatic ions (AIs), no collisions, spanned  $0.01 < k_y \rho_e < 0.31$  with 32 modes, ran to  $t \sim 300 a/v_{te}$  and used plasma parameters:  $\rho = \psi_n = 0.4$ ,  $r/a = 0.566$ ,  $r/R = 0.35$ ,  $q = 1.35$ ,  $\hat{s} = (\rho/q)(dq/d\rho) = 0.29$ ,  $\beta_e = 0.049$ ,  $T_e = 0.59$  keV,  $(1/T_e) dT_e/d\rho = -2.04$ ,  $n_e = 4.4 \times 10^{19} \text{ m}^{-3}$ ,  $(1/n_e) dn_e/d\rho = 0$ . The predicted  $\chi_e$  values with a range of domain sizes and resolutions, with/without kinetic ions (KIs) and electron collisions, were consistent to within a factor of around 2 [7]. Here we probe further the robustness of this very important conclusion with longer GS2 simulations that include kinetic ions, collisions and equilibrium flow shear. Despite the large impact of magnetic perturbations (especially  $\delta B_{\parallel}$ ) on linear ETG growth rates [18], the saturated electron heat fluxes  $q_e$  in electrostatic and electromagnetic simulations were similar and predominantly due to electrostatic fluctuations [7, 32]. For reasons of economy with computing resources, most of the GS2 simulations reported here are electrostatic, although a subset of key results was checked and found to be consistent with fully electromagnetic simulations.

Recent longer ETG simulations, to  $t \sim 1500 a/v_{te}$ , with an electrostatic version of the AI model of [7], lead at long times to the runaway growth of  $q_e$  that is illustrated in figure 3(a). At late times the  $\Phi$  spectrum becomes dominated by a single  $k_x = 0$  mode at low  $k_y$ , and this may be associated with a slowly growing mode close to the edge of the spectral domain. A similar phenomenon in previous AI ETG simulations, for a large aspect ratio equilibrium, was cured by including kinetic ions [33], but in our case this merely delayed the onset of the unresolved dominant mode. Figure 3(a) also shows that when the collisionless AI simulation is continued from  $t \sim 1500 a/v_{te}$  with the typical level of equilibrium flow shear at mid-radius in MAST ( $\gamma_E = 0.005 v_{te}/a$ ), the simulation quickly recovers from what appeared a catastrophically unresolved situation; and including electron collisions (at the experimental level) in the AI model cures the saturation problem and considerably improves the convergence of the spectrum (the same is true for the KI model). The healing of the simulation, with the addition either of electron collisions or flow shear, is probably due to the stabilization of

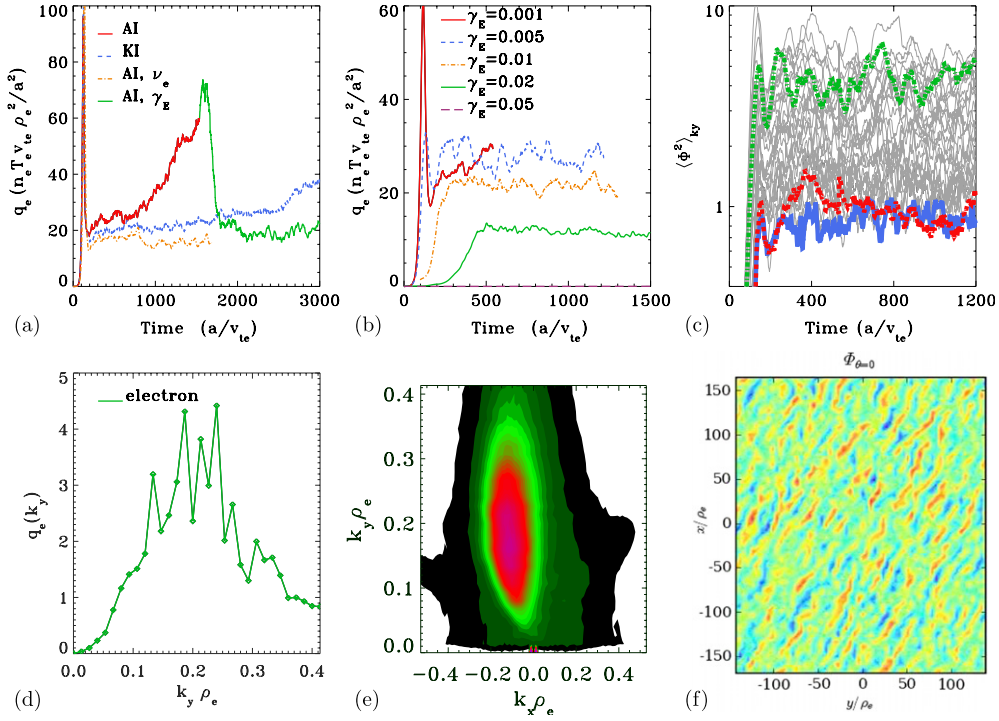


**Figure 3.** (a)  $q_e$  versus  $t$  with collisionless AI and KI, AI with collisions and collisionless AI with  $\gamma_E = 0.005$ . (b)  $q_e$  versus  $t$  for various  $\gamma_E$  for the Miller equilibrium with  $L_y = 75\rho_e$  and  $J_{\text{twist}} = 4$ . For the  $\gamma_E = 0.005$  case in (b): (c)  $\langle \Phi^2 \rangle_{k_y}$  versus  $t$ , where red dotted, green dash-dotted and blue solid curves correspond to the lowest, middle and highest  $k_y$  and (d)  $k_y$  spectrum of electrostatic contribution to  $q_e$  at  $t = 1200$ . For the  $\gamma_E = 0.02$  case in (b): (e) time ( $1000 < t < 2000$ ) and field line averaged spectrum of  $\langle \Phi^2 \rangle(k_x, k_y)$  and (f)  $\Phi$  contours at the outboard midplane, for  $t = 2000$ . (All times and frequencies are normalized to  $a/v_{te}$  and  $v_{te}/a$ , respectively.)

weakly unstable trapped electron driven modes in the region  $k_y \rho_i \sim 1$ , as discussed at the end of [appendix A](#). GYRO simulations have also found that flow shear helps in resolving ETG turbulent saturation with the AI model [34].

The electron heat flux,  $q_e$ , varies by less than a factor 2 in simulations with different perpendicular domain sizes: e.g. the flux tube extent in the binormal direction at the outboard midplane,  $L_y$ , was varied in the range  $50 < L_y/\rho_e < 100$ ; and the radial size,  $L_x$ , determined by the parameter  $J_{\text{twist}}$  with  $L_x = J_{\text{twist}} L_y / (2\pi \hat{s})$ , was set using  $J_{\text{twist}} = 2$  and 4. Linear and nonlinear simulations using both numerical and Miller [35] equilibria give consistent results. Artificial scans in  $\gamma_E$ <sup>10</sup>, both using initial conditions with low amplitude noise (see figure 3(b)), and restarting from the saturated state of a resolved simulation with collisions and  $\gamma_E = 0$ , find that ETG turbulence is suppressed at  $\gamma_E \sim 0.05 v_{te}/a$ , which is an order of magnitude larger than the typical mid-radius equilibrium flow shear in MAST ( $\gamma_E^{\text{exp}} \sim 0.005 v_{te}/a$ ) and is close to  $\gamma_{\text{max}}$  ( $\gamma_{\text{max}} = 0.04 v_{te}/a$ ). The steady and well resolved spectrum of  $\Phi$  in the AI simulation with electron collisions and  $\gamma_E = 0.005 v_{te}/a$  is illustrated in figure 3(c). Figure 3(d) shows the corresponding clearly resolved peak in the  $k_y$  distribution of the electrostatic contribution

<sup>10</sup> The linear drive term had a negligible impact on ETG turbulence in GYRO simulations for MAST [36], and was excluded from these GS2 studies of the effect of flow shear on ETG turbulence.  $qR/r \sim 4$  on this MAST surface, and so the linear drive term should be small.

to  $q_e$ . The shearing of radially extended ETG streamer structures for the  $\gamma_E = 0.02v_{te}/a$  case is evident both in the time and field line averaged spectrum  $\langle \Phi^2 \rangle(k_x, k_y)$ , and in the outboard midplane contour plot of  $\Phi$ , shown in figures 3(e) and (f). Turbulence suppression arises at slightly lower  $\gamma_E$  in fully electromagnetic simulations, where including  $\delta\mathbf{B}$  gives a lower  $\gamma_{\max} = 0.025v_{te}/a$ .

Complementary local simulations of ETG turbulence were performed with GYRO for MAST-like parameters, including flow shear and kinetic ions [36]. These simulations investigated GYRO's non-periodic radial boundary conditions, demonstrated quantitative convergence with grid size and resolution and predicted an experimentally significant level of electron heat transport arising from ETG turbulence at mid-radius. The simulated electron thermal diffusivity ( $\chi_e^{\text{sim}} \sim 2\text{--}4 \text{ m}^2 \text{ s}^{-1}$ ) was found to be comparable to the typical experimental value ( $\chi_e^{\text{exp}} \sim 2\text{--}5 \text{ m}^2 \text{ s}^{-1}$  [10]), and consistent with results from GS2 shown above and previously [7]. Additional GYRO runs demonstrated that ETG transport is sensitive to  $q$  and  $\hat{s}$ , which vary widely across ST plasmas.

In this section we have presented simulations, which run to long times and include the physics of collisions, kinetic ions and sheared toroidal equilibrium flow, that add weight to the conclusion from [7] that ETG turbulence can carry significant electron heat transport at mid-radius in MAST.

## 5. Conclusions

Sheared toroidal equilibrium flows can be sufficiently large to suppress ITG turbulence in STs, and this must significantly affect their energy confinement. Such flows can readily be accommodated within the gyrokinetic framework for  $V \sim O(M_\phi v_{ti})$ , for  $1 > M_\phi > \rho_i/a$ , and affect turbulence through two mechanisms: the sheared perpendicular component of the toroidal flow acts to suppress the transport from microturbulence, but the radial shear in the parallel component of the equilibrium toroidal flow provides a linear drive that can enhance turbulence. The strength of the linear drive relative to the perpendicular shearing term is  $\propto (qR/r)B_\phi/B$ , which corresponds at large aspect ratio to  $B_\phi/B_p$ . Turbulence is more strongly suppressed when this factor is reduced, as is naturally achieved both at high plasma current and at mid-radius in the ST. We can therefore expect STs to provide a favourable environment for turbulence suppression through sheared toroidal flow.

Sheared toroidal flow has recently been implemented and tested in two local flux-tube gyrokinetic codes (GS2 and GKW). Linear gyrokinetic simulations using GS2, including equilibrium flow shear at the approximate level realized in the MAST experiment, demonstrate that ITG modes can indeed be suppressed while ETG modes remain unstable. Nonlinear ETG turbulence simulations have been presented for conditions typical of mid-radius in MAST, and show that both collisions and modest equilibrium flow shear can sharpen the low  $k_y$  cut-off to significantly improve the resolution of the saturated turbulence. In numerical experiments with artificially raised levels of  $\gamma_E$ , it is found that the ETG turbulence only starts to be diminished as  $\gamma_E$  approaches the value of the maximum linear ETG growth rate. These results add weight to the main conclusion of [7] that ETG induced transport can be significant at mid-radius in MAST.

Flows in MAST are close to sonic, with  $M_\phi \sim 0.4$ , and to improve current GK simulations it will be necessary in the future to include, self-consistently with the flow shear, the finite  $M_\phi$  corrections to the GKE. In the co-rotating frame these corrections appear as a Coriolis force (which is included in GKW [37]) and a centrifugal force.

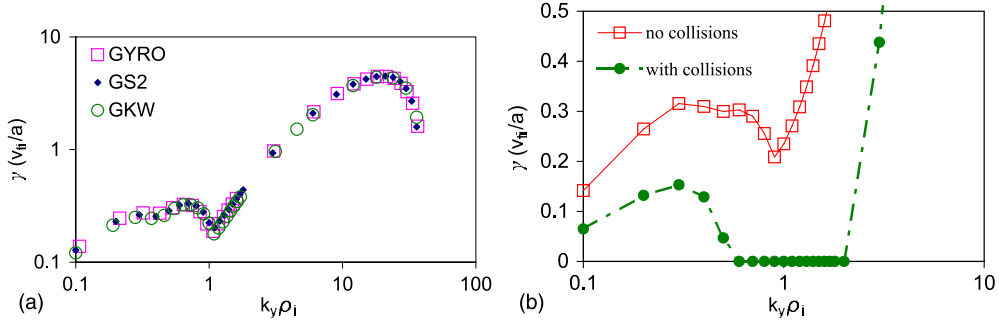


**Figure A1.**  $\gamma$  normalized to  $v_{ti}/a$  versus  $k_y \rho_i$  for linear electrostatic calculations with kinetic electrons for the MAST equilibrium described: (a) without collisions from GS2, GKW and GYRO and (b) with and without collisions from GS2.

## Acknowledgments

The authors are very grateful to Alberto Bottino, Jeff Candy, Joachim Hein, Gavin Pringle, Gary Staebler, Ron Waltz and Michele Weiland for many helpful discussions. Supercomputing access was used to perform some of the reported simulations: they thank EPSRC for access to HECToR, and the DEISA Consortium ([www.deisa.eu](http://www.deisa.eu)), co-funded through the EU FP6 project RI-031513 and the FP7 project RI-222919, for support within the DEISA Extreme Computing Initiative. This work was funded partly by the UK Engineering and Physical Sciences Research Council and by the European Communities under the contract of association between EURATOM and UKAEA, in part by the Leverhulme Trust Network for magnetized plasma turbulence, and A Schekochihin was partly supported by STFC. The views and opinions expressed herein do not necessarily reflect those of the European Commission.

## Appendix A. Comparing electrostatic microstability analyses from local GK codes for a MAST equilibrium

We have compared linear results from the local gyrokinetics codes GKW, GS2 and GYRO, using parameters of a strongly shaped equilibrium flux surface in the MAST H-mode discharge #8500 [10, 18]:  $\rho = r/a = 0.7$ ,  $r/R = 0.443$ ,  $q = 2.1$ ,  $\hat{s} = (\rho/q)(dq/d\rho) = 2.2$ ,  $\beta = 0.06$ ,  $T_i = 0.385$  keV,  $(1/T_i)dT_i/d\rho = -4.39$ ,  $T_e = 0.346$  keV,  $(1/T_e)dT_e/d\rho = -2.79$ ,  $n_e = 5.7 \times 10^{19} \text{ m}^{-3}$ ,  $(1/n_e)dn_e/d\rho = -0.44$ , elongation  $\kappa = 1.56$ ,  $d\kappa/d\rho = 0.5$ , triangularity  $\delta = 0.2$ ,  $d\delta/d\rho = 0.43$  and  $(1/a)dR/d\rho = -0.29$ . Figure A1(a) demonstrates good agreement between the computed spectra of the dominant linear growth rate for a collisionless electrostatic model with kinetic electrons and without flow shear.

Figure A1(b) shows, from GS2 runs using a local Miller parametrization of the equilibrium [35], that with collisions the modes around  $k_y \rho_i \sim 1$  become stable. Estimating the ratio of the electron detrapping frequency to the diamagnetic frequency, for these parameters, gives  $\nu_{\text{detrapp}}^e/\omega_* \gtrsim 1$  for  $k_y \rho_i \sim 1$ , which is consistent with a reduced trapped electron drive around this wavenumber.

Euratom © 2009.

## References

- [1] Akers R J *et al* 2008 Transport studies in the MAST spherical tokamak *Proc. 22nd IAEA Fusion Energy Conf. (Geneva, Switzerland)* EX2-2

- [2] Kaye S M *et al* 2007 *Nucl. Fusion* **47** 499
- [3] Biglari H, Diamond P H and Terry P W 1990 *Phys. Fluids B* **2** 1
- [4] Waltz R E, Kerbel G D and Milovich J 1994 *Phys. Plasmas* **1** 2229
- [5] Kotschenreuther M, Rewoldt G and Tang W M 1995 *Comput. Phys. Commun.* **88** 128
- [6] Peeters A G and Strinzi D 2004 *Phys. Plasmas* **11** 3748
- [7] Joiner N *et al* 2006 *Plasma Phys. Control. Fusion* **48** 685
- [8] Wakatani M *et al* 1999 *Nucl. Fusion* **39** 2175
- [9] Valovic M *et al* 2009 *Nucl. Fusion* **49** 075016
- [10] Field A R *et al* 2004 Core heat transport in the MAST spherical tokamak *Proc. 20th IAEA Fusion Energy Conf. (Vilamoura, Portugal)* EX/P2-11
- [11] Roach C M *et al* 2008 *Nucl. Fusion* **48** 125001
- [12] Staebler G M, Kinsey J E and Waltz R E 2005 *Phys. Plasmas* **12** 102508
- [13] Staebler G M *et al* 2008 Testing the trapped gyro-landau fluid transport model with data from tokamaks and spherical tori *Proc. 22nd IAEA Fusion Energy Conf. (Geneva, Switzerland)* TH/P8-42
- [14] Jolliet S *et al* 2007 *Comput. Phys. Commun.* **177** 409
- [15] Kotschenreuther M *et al* 2000 *Nucl. Fusion* **40** 677
- [16] Candy J and Waltz R E 2003 *J. Comput. Phys.* **186** 545
- [17] Applegate D J *et al* 2004 *Phys. Plasmas* **11** 5085
- [18] Roach C M *et al* 2005 *Plasma Phys. Control. Fusion* **47** B323
- [19] Applegate D J *et al* 2007 *Plasma Phys. Control. Fusion* **49** 1113
- [20] Vermare L *et al* 2008 *J. Phys. Conf. Ser.* **123** 012040
- [21] Told D *et al* 2008 *Phys. Plasmas* **15** 102306
- [22] Wong K L *et al* 2008 *Phys. Plasmas* **15** 056108
- [23] Stutman D *et al* 2009 *Phys. Rev. Lett.* **102** 115002
- [24] Artun M and Tang W M 1994 *Phys. Plasmas* **1** 2682
- [25] Hammett G W *et al* 2006 Implementation of large scale  $E \times B$  shear flow in the GS2 gyrokinetic turbulence code *48th Annual Meeting of the Division of Plasma Physics (American Physical Society) (Philadelphia, Pennsylvania, USA)* abstract VP1.136
- [26] Connor J W, Taylor J B and Wilson H R 1993 *Phys. Rev. Lett.* **70** 1803
- [27] Waltz R E, Dewar R L and Garbet X 1990 *Phys. Plasmas* **5** 1784
- [28] Kinsey J, Waltz R E and Candy J 2005 *Phys. Plasmas* **12** 062302
- [29] Dimits A M *et al* 2000 *Phys. Plasmas* **7** 969
- [30] Peeters A G and Angioni C 2005 *Phys. Plasmas* **12** 072515
- [31] Catto P J, Rosenbluth M N and Liu C S 1973 *Phys. Fluids* **16** 1719
- [32] Joiner N J 2005 Microinstabilities in spherical tokamaks *PhD Thesis* Imperial College, London
- [33] Nevins W M *et al* 2006 *Phys. Plasmas* **13** 122306
- [34] Candy J *et al* 2007 *Plasma Phys. Control. Fusion* **49** 1209
- [35] Miller R L *et al* 1998 *Phys. Plasmas* **5** 973
- [36] Guttenfelder W *et al* 2009 Gyrokinetic simulations of electron scale turbulence in spherical tokamak plasmas with flow shear *36th EPS Conf. on Plasma Physics (Sofia, Bulgaria)* P-4.115
- [37] Peeters A, Angioni C and Strintzi D 2007 *Phys. Rev. Lett.* **98** 265003